Journal of Materials Chemistry B

Accepted Manuscript

ROYAL SOCIETY OF CHEMISTRY

www.rsc.org/materialsB

Journal of Materials Chemistry B

ARTICLE

Dynamically tunable polymer microwells for directing mesenchymal stem cells differentiation into osteogenesis

Received 00th January 20xx,
Accepted 00th January 20xx

DOI: 10.1039/x0xx00000x

www.rsc.org/

Tao Gong†, Liuxuan Lu†, Dian Liu†, Xian Liu†,#, Kun Zhao†, Yuping Chen†, Shaobing Zhou†*

Directing stem cells towards a desired location and function by utilizing the structural cues of biomaterials is a promising approach for inducing effective tissue regeneration. Here, we exploited the dynamic structural signals resulting from the micro-well substrates to guide the rat bone marrow mesenchymal stem cells (rBMSCs) to differentiate along osteogenesis. The micro-well substrates were fabricated via thermal lithography with arrays of triangle-, square-, hexagon- or round-shaped micro-wells, which were made of biocompatible and biodegradable polymer network containing six-arm poly(ethylene glycol)-poly(ε-caprolactone) (6A PEGPCL) with excellent thermally activated shape memory function. The dynamically tunable geometric microwells and the resulting mechanical force effectively and significantly regulated the cytoskeletal structure and tension of rBMSC in vitro without induction media when compared with the static patterned. Cellular and molecular analyses revealed that cells cultured in various dynamic micro-wells had disparately differentiated along adipogenesis and osteogenesis pathways. We further implanted these dynamically tunable geometric micro-well substrates into the site of rabbit mandible defect and found that they prompted differentiation of mesenchymal stem cells into osteogenesis and in turn efficiently repaired the mandible bone defect. Taken together, this work points to the role that dynamic geometric shape cues can orchestrate the mechano-chemical signals thus direct MSCs to appropriate fates.

1. Introduction

Mesenchymal stem cells (MSCs) hold great potential for regenerative medicine and tissue-engineering. These cells in situ, within organs or tissues, are embedded into a highly structured and mechanically dynamic microenvironment.[1-4] Their functions and fates are strongly influenced by environmental factors such as physical signals, including topological and mechanical cues from the extracellular matrix (ECM).[5-10] The topography of cell culture biomaterials (substrates), particularly of the micropatterned surfaces mimicking the stem cell microenvironment, has been evidenced in many previous studies to influence cell shape, spreading, migration, and even differentiation.[11-17] However, these synthetic topographical features are almost studied in a static mode, which do not truly simulate the naturally dynamic microenvironment of stem cells. Lu et al. reported that the dynamic of cellular responses to changes in the microenvironment is also a fundamental property of living systems, ensuring the functional and mechanical coherence of tissues during development or renewal.[18, 19] Therefore, it remains a great challenge for stem cell researchers to use biomaterials to further mimick stem cell microenvironments and thus facilitate definite differentiation of stem cell for their application in regenerative medicine.

To address this challenge, one effective strategy is to exert an external mechanical force onto the biomaterial substrate and then dynamically change its topographical features. The forces externally applied to the extracellular environment have been shown to alter stem cell differentiation before.[4, 8, 20-22] Living cells can actually sense the mechanical forces, convert them into biological signals, and then alter their shapes and functions correspondingly.[23,24] The mechanical deformation can be translated into biochemical response, and cytoskeletal tension may be a driving factor in stem cell differentiation.[11, 25, 26] In a recent key study, MSCs were induced to distinctly differentiate to myogenic pathway when cultured on the substrates with the uniaxial strain but along osteogenic pathway with uniform biaxial stretch, marking the importance of external stresses in MSC differentiation.[27, 28]

E-mail: shaobingzhou@hotmail.com
† Key Laboratory of Advanced Technologies of Materials, Ministry of Education, School of Materials Science and Engineering, Southwest Jiaotong University, Chengdu 610031, China
# State Key Laboratory of Oral Diseases, West China Hospital of Stomatology, Sichuan University, Chengdu, China
DOI: 10.1039/x0xx00000x

The shear stresses and tensile loads are often employed as mechanical forces.[23, 29, 30] However, these external forces are so complex that it is very difficult to manipulate and precisely control them. Stimuli-responsive polymer actuators, which have the ability to respond to external stimuli, were used to exert the mechanical forces to overcome this limitation.[29] Among these actuators, electroactive polymer comprised of conductive nanomaterials emerged as a good example due to its ability to change the size or shape under electrical stimulations and produce a mechanical force as a consequence.[31, 32] Unfortunately, the conductive nanomaterials such as metal nanoparticles and carbon nanostructures are generally toxic to cell growth. Most recently, shape memory polymers (SMPs) has been proposed as a possible solution to current limitations since they can change their permanent shape into a temporary shape, and recover to their permanent shape upon application of an appropriate stimulus such as temperature.[33, 34] Therefore, during the shape recovery process, a resultant stress is released automatically from the polymer and can be used to mimick the naturally dynamic microenvironment of stem cells. The incorporation of the mechanical force and topographical feature to form a dynamic microenvironment may be the most effective approach to precisely guide stem cell differentiation towards the desired cell lineages.

Previously, we have confirmed that 6-arm PEG-PCL polymer possessed excellent thermally activated shape memory function after photo-crossslinked.[35] In this work, we present a novel method to decouple the multiple physical signals including geometrical shape of substrate, and dynamic force in determining MSC lineage commitment as shown in **Figure 1**. A series of polymer substrates with various geometrical shapes are programmed through thermal embossing micro-imprint lithography. These substrates can be deformed by stretched at a high temperature and then cooled down under a fixed strain to memorize the temporary shape by locking the deformed polymer chains, and later recover to the original shape by heating, again. Here, this shape memory effect provides a programmed control of both the dynamic change of the surface topography (**Figure 1D**) and a dynamic local force, which is released from the polymer when shape is changed from the surface transformation between different geometrical shapes. The programmed control of the dynamic change of the surface topography is through adjusting the gradient recovery temperature. Thus, by simply changing the environmental temperature, the surface micropatterns can be changed dynamically and in turn a dynamic local force on these substrates is generated automatically, which can be further used to stimulate stem cells response and direct their fates.

2. Experimental Section

2.1 Materials

ε-Caprolactone (ε-CL, 99.9%, Aldrich) were distilled over freshly powdered CaH_2 under a reduced pressure. 6-arm polyethylene glycol (6A PEG, Mn≈6000) was purchased from Liming Research Institute of Chemical Industry in Luoyang (China). Diphenyl (2, 4, 6-trimethylbenzoyl) phosphine oxide (TPO) and stannous chloride ($SnCl_2$) were purchased from Biokem Technology Co., Ltd (China). All other chemicals and solvents were of reagent grade or better.

2.2 Fabrication of the microwells

6A PEG-PCL-AC was synthesized as described in our previous reports.[35, 36] The microwells were fabricated on the surface of the polymer substrate through thermal micro-imprint lithography as displayed in **Figure 1A**. We fabricated silicon microbump structures (Triangle, Square, Hexagon and Circle) with area about 2000 μm^2 and height of 5 μm. The completely dried 6A PEG-PCL-AC/TPO was kept in an oven at 60 ℃ to make it melt. Then, the molten mass was placed on the silicon template and the silicon template was sequentially heating for another 30 min at 60 ℃ to acquire 6A PEG-PCL-AC/TPO polymer substrates with designed microwells. Photo-crosslinking of 6-arm PEG-PCL-AC/TPO was initiated by the UV light (λ = 360 nm) generated from a high-intensity long wave UV lamp (100 W, intensity: 400 μW cm^{-2}) for 40 min. Static tensile test was accomplished at the cross-head speed of 0.5 mm min^{-1} at 35, 38 and 41 °C, respectively, using a universal testing machine Instron 5567 (Instron Co., Massachusetts). The degradation of polymer meshes was performed as below. The dried 6A PEG-PCL-AC meshes were cut into small square pieces. Each cut specimen was exactly measured for initial weight (50 mg) and immersed in 25.0 mL of phosphate-buffered saline (PBS, 0.1 M , pH 7.4) in test tubes. The mass loss was determined gravimetrically by comparing the dry weight remaining at a specific time with the initial weight. The molecular weight was determined using GPC.

2.3 Characterization of the macroscopic and microcosmic shape memory effect

The triple shape memory effect was measured by using a controlled force mode on a Dynamic mechanical analysis (DMA, TA, DMA-Q 800) according to a typical investigation procedure.[37] First, samples were heated to 60 ℃ for 1 min. Second, the 1.2 MPa stress was loaded at a certain rate and then cooled to the deformation temperature 0 ℃ at 1.2 MPa. Then, the stress unloaded back to 0 MPa at 0 ℃. Finally, the shape memory process was measured with the temperature increased from 0 ℃ to 32 ℃, 35 ℃, 38 ℃ and 41 ℃. The temperature was equilibrated at 32 ℃, 35 ℃, 38 ℃ and 41 ℃ for 3 min, respectively. All of the shape memory processes were repeated two times. The ribbon- samples were deformed from the unbent to a helical shape at 60 ℃, and fixing the helical shape for 5 min at 0 ℃. The microwells surface was deformed from the original shape to temporal shape by stretching the substrate, and was also cooled to fix the deformed shape (**Scheme S1** in Support Information (SI)). Both of the macroscopical and microscopical shape memory recovery processes were heated from 35℃ to 38 ℃ and 41 ℃ based on the DMA results. The morphology of the microwells and dynamic change of the microwells were mainly analyzed by Scanning electron microscope (SEM, S-3500, Hitachi Instruments, Tokyo, Japan). The shape recovery ratio (R_r) and shape fixed ratio (R_f) were calculated according to the equations below:

$$R_f = \frac{\varepsilon_{S1}}{\varepsilon_{S1,F}}$$

$$R_r = \frac{\varepsilon_{S1,F} - \varepsilon_{Sx,rec}}{\varepsilon_{S1,F}}$$

Where $\varepsilon_{Sl,F}$ is the maximum strain during deformation, ε_{Sl} is the retention strain at 0 ℃, and $\varepsilon_{Sx,rec}$ is the strain during recovery process.

2.4 Cell culturing and micropatterning of rBMSCs

The c-6A PEGPCL films with different microwells were cut into flakes with size 8×8×2 mm (length × width × thickness), and then sterilized with ethanol and overnight ultraviolet irradiation before cell seeding. Here, the typical classes of temporary surface patterns were fabricated. The surface micropatterns on c-6A PEGPCL substrate were stretched and deformed to the 200% at 45 °C with a tensile stress of 1 MPa, and then cooled to 0 °C to fix the deformed shape. The sample, which was not deformed after stripped from the Si template, is defined to the static (original shape) group; and the sample stretched and fixed but not recovered at 38 ℃and 41 ℃is defined to the static (temporary shape) group. rBMSCs were obtained from 10-d-old newborn rat by whole bone marrow culture method.[38] The rBMSCs were grown in Dulbecco's Modified Eagle's Medium-low glucose (DMEM-LG, Hyclone) with 10% fetal bovine serum (FBS, Gibco, GB) at 37 ℃. Then, the cells with a density of 5×10^3 cells/well were cultured on the different surfaces at 35 ℃ for two days. For the dynamic programmed surface recovery, the plates were transferred to 38 ℃ and 41 ℃ incubator for 1 hour on day 2 and day 4, respectively. After heat treatment, the plates were then back to 35 ℃ incubator. Alamar blue assay was carried out for cell proliferation on different surfaces during the dynamic culture. At pre-designed time points of 2, 4, and 6 days, the medium was remove and 300 μl Alamar blue solution (80% media 199, Gibcos,10% Alamar blue (Biosource, Nivelles, Belgium), and 10% FBS; V/V) were added to each well. Finally, 200 μL Alamar blue solution from each samples were transferred to a 96-well plates and read at 570 nm (excitation)/600 nm (emission) in a ELISA microplate reader (Molecular Devices, Sunnyvale, CA). Results were the mean ± standard deviation of three times. CCK8 (Dojindo) assay was carried out for cell proliferation on different surfaces during the dynamic culture. CCK8 from each samples were transferred to 96-well plates and read at 480 nm (emission) in an ELISA microplate reader (Molecular Devices, Sunnyvale, CA). Cytochalasin D (0.2 μM) added to cell culture were determined empirically to allow complete spreading with no visually apparent changes to morphology.

2.5 Immunostaining and western blotting

Cell morphology and cytoskeleton on the different surfaces were observed by confocal laser scanning microscope (CLSM, FV1000, Olympus, Japan). After fixated by 2.5% glutaraldehyde overnight, the cells on the substrate stained by 4',6-diamidino-2-phenylindole (DAPI, Sigma, USA) and Rhodamine-phalloidin (Sigma, USA) for nuclei and F-actin, respectively. Immunofluorescence technique was used to detect the osteogenesis protein OCN (Rabbit Anti-

OCN, 1:200, Beijing Biosynthesis Biotechnology Co., LTD) in dynamic culture. Alexa Fluor secondary antibodies 488 goat anti mouse IgG (1:200, Beijing Biosynthesis Biotechnology Co., LTD) are used for detection. For western blotting analyses, cell lysates were pooled from cells on 6 sheets and 100 μg cell lysates were subjected to 7.5% gel electrophoresis after 14 days cultured (1:1000 anti-ROCK1 and 1:5000 anti-GAPDH (Beijing Biosynthesis Biotechnology Co., LTD). The membranes were marked with dilution of secondary antibodies (horseradish per-oxidase). Protein bands were visualized by using the ECL detection system (Thermo), and intensity of bands was quantified by using Image J. At least three times were carried and quantified for analysis.

2.6 RNA Isolation and reverse transcription-polymerase chain reaction

The control groups contain the static original geometrical shape and the static temporary geometrical shape (after deformation but not recovery). The microwells surface was deformed from the original shape to temporal shape by stretching the substrate, and was also cooled to fix the deformed shape (**Scheme S1** in SI). For reverse transcription-polymerase chain reaction, the rBMSCs with a density of 5×10^3 cells/well were cultured on the different surfaces and cultured for 14 days without addition of induction medium. After cell cultured and collected, total RNA was extracted from all the specimens using the TRIzol Reagent (Life Technologies, Rockville, MD), cDNA synthesis was performed with RevertAid First Strand cDNA Synthesis Kit (Thermo, USA). The qPCR reactions were performed with initial incubation at 95 ℃ for 5s followed by 55℃ for 30 s and 72℃ for 30s. The relative expression level of each miRNA was normalized to the level of GAPDH mRNA and calculated using the ΔΔCT method. The products were resolved by 2% agarose gel electrophoresis in trisborate/ethylenediaminetetraacetic acid (EDTA) buffer and visualised by staining with ethidium bromide. Gene primers used for real-time PCR were: Runt related transcription factor 2 (RUNX2); osteopontin (OPN); osteocalcin) (OCN); peroxisome proliferator-activated receptors γ (PPARγ); leptin (LEPTIN); glycerol-3-phosphate dehydrogenase (GPDH). BLAST was used to search for all primer sequences to ensure gene specificity. For rBMSCs osteogenesis induction culture, the rBMSCs were cultured for 8 days with the differentiation media including 45% Hank's F12 , 45% α-MEM, 10% FBS , 50 μM ascorbate-2-phosphate , 10 mM β-glycerol phosphate, 100 nM Dexamethasone. The adipogenic induction media including High Glucose DMEM, 10% FBS, 1 μ M Dexamethasone, 10 μ g/ml insulin , 200 μ M indometacin and 0.5 mM IBMX.

Gene	Primers
RUNX2	5′-GCT TCT CCA ACC CAC GAA TG-3′ 5′-GAA CTG ATA GGA CGC TGA CGA-3′
OCN	5′- AAA CAT GGC AAG GTG TGT GA-3′; 5′- AGG TGA CCA GGA CGT TTT TG-3′;
OPN	5′- AAG CCT GAC CCA TCT CAG AA-3′; 5′- GCA ACT GGG ATG ACC TTG AT-3′;
PPARγ	5′-AAG ACC ACT CCC ACT CCT TTG-3′; 5′ -GTC AGC GGA CTC TGG ATT CA-3′
LEPTIN	5’ -CTG AAG ACA CAG CTG AGG AC-3′ ′; 5’ -CTG GTG AAT GTG TGT AAG AC-3’
GPDH	5′- ATC AAG GGA AAG CAG GAA GC-3′; 5′- CCT TGT CTA CAG GTG CAT CA-3′

2.7 In vivo animal experiment and surgical procedures.

The static and dynamic microwell films were cut out into a piece of circle shape (diameter × thickness, 8mm×1mm) prior to *in vivo* use. All of the animals in this study were cared for according to the protocol approved by the Animal Care Committee of Sichuan University. Rabbits were anesthetized via intravenous administration of Pentobarbitol Sodium (30 mg/kg) prior to all experimental procedures. A total of 12 New Zealand white rabbits were randomly divided into two groups: static microwells group, dynamic microwells group. Two of these groups were randomly applied on two sides of one rabbit mandible. One film group was inserted into one side of the mandibular defect, while another film group was implanted on the other side of the defect. The bone defects were performed according to previous reports.[39] Briefly, a 2 cm incision was made approximately 1 cm lower from the edge of the mandible body to expose the bone. Next, a dental drill was used to make the critical-sized bone defects (CSD) with a diameter of 8 mm on both sides of the mandible body, and the periosteum was removed during this process. The incision was closed in layers using 4-0 resorbable sutures. These animals received prophylactic i.m. antibiotic at the time of surgery and for 3 days postoperatively. All rabbits were sacrificed after a recovery period of 8 weeks following histological examination.

2.8 Histological examination

After the rabbits were sacrificed at 8 weeks, the other half of the samples from each group were fixed in 4% paraformaldehyde solution for histological examination. The samples were dehydrated with alcohol and embedded in methylmethacrylate without decalcification. A model SP1600 microtome (Leica Micro-systems, Wetzlar, Germany) was used to cut the sections at a thickness of 100 μm and polished to approximately 15-20 μm for trichrome-masson staining. A microscope (DF 490, Leica, Switzerland) was used to examine the histological images, and images were captured using imaging software (Leica). The ratios between the mineralized new bone area and the total defect area of the images were calculated.

2.9 Statistical analysis

All data were expressed as mean ± SD. A probability value (p) of less than 0.05 was determine

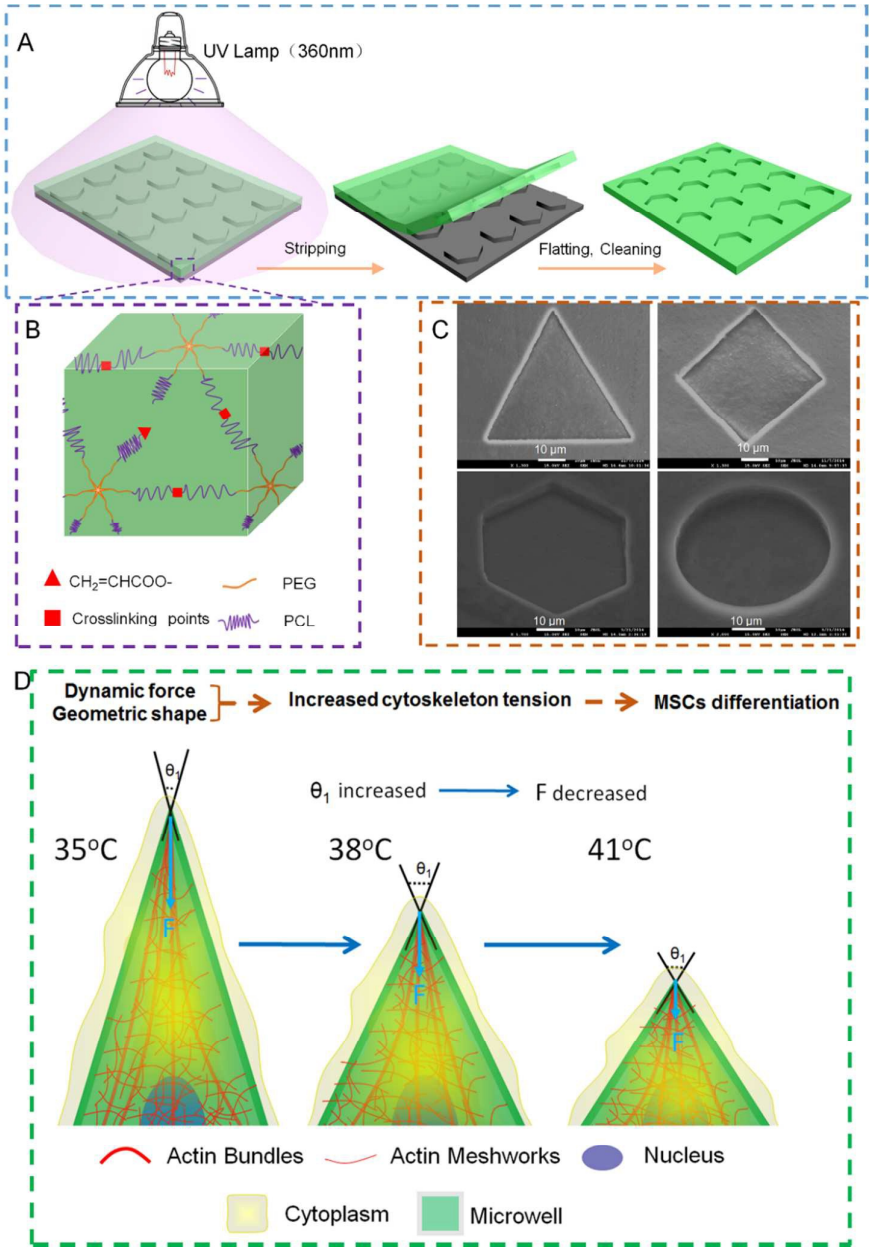

Figure 1. (**A**) Scheme of engineering of the c-6 A PEGPCL substrate with Hexagon (area: 2000 μm^2, depth: 5 μm) and (**B**) The chemically cross-linked molecular structure of c-6 A PEGPCL shown in the panel. (**C**) Topographic surface images of the c-6 A PEGPCL substrate with various microwells observed by SEM. (**D**) Schematic illustrating how cytoskeletal organization affected by the dynamic microwells.

statistical significance of the data.

3. Results and discussion

3.1. Synthesis of the microwells

Figure 1A&B shows the synthesis process of the microwells. When the molten 6A-PEGPCL-AC was pouring on the silicon microbump substrate and exposed to UV irradiation, the phosphine oxide decomposed into free radical and trigger the free radical polymerization of AC to form the cross-linked network. The formation of cross-linked structure confers excellent shape memory effect on a surface microwells. **Figure 1C** shows topographic surface images observed by SEM. These surface microwells are regular triangle, square, regular hexagon, and circle shape. The area of these surface microwells is 2000 μm^2, and the depth is 5 μm. Here, this triple shape memory function provides a programmed control of both the dynamic change of the microwells geometry (**Figure 1D**) and a dynamic local force. The dynamic local force as an external mechanical force can be controlled easily, which is employed to control the rBMSCs differentiation in this study.

3.2. The macroscopic and microcosmic shape memory effect of the microwells

To confirm whether the c-6A-PEGPCL has a good shape memory effect (SME) within the limits of the body temperature, a cyclic tension experiment was carried out. The cyclic curve includes four steps: 1) the c-6A PEGPCL film was stretched under a 1.2 MPa mechanical stress at 60 ℃; 2) fix the deformed shape at 0℃ (R_f = 96.4%); 3) after fixed shape, unloading the stress ; 4) with the temperature gradient increased to 50℃, the temporary shape convert back into the original shape. As shown in **Figure 2A&B**, when the temperature was gradient increased to 41 ℃, the triple shape memory effect was observed. When the temperature increased from 35℃to 38℃, 41℃, the R_r increased from 0% to 52.1% (T_{r1}), and 92.4% (T_{r2}), respectively. **Figure 2C**

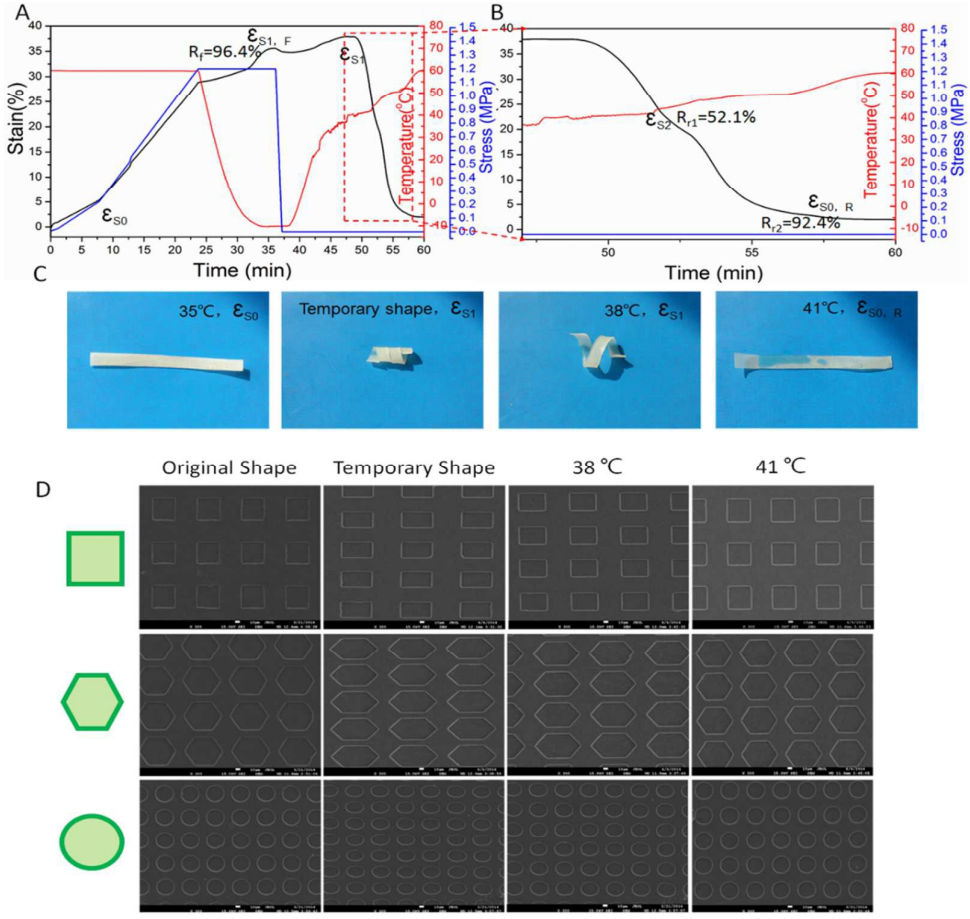

Figure 2. (**A**) and (**B**) Quantitative thermal mechanical cycle of c-6 A PEGPCL (T_d=60℃, T_{r1}=38℃, T_{r2}=41; R_f =94.2%, $R_{r2}(S_1 \rightarrow S_2)$= 54.1%, $R_{r3}(S_2 \rightarrow S_3)$= 92.4%). (**C**) Visual demonstration of the shape memory recovery. S_0: initial shape, S_1: temporary shape (35 ℃) which is folded at 60 ℃ and fixed at 0℃, S_2: the first temporary shape (38 ℃); $S_{0,R}$: the recovered shape (41 ℃). (**D**) Topographic surface images of the c-6 A PEGPCL substrate with varies microwells observed by SEM before and after shape-memory transition by a 38℃ and 41℃ heat treatment (Scale bar: 10 μm).

gives series of photos of the macroscopic triple shape-recovery process of the c-6A PEGPCL at 35 ℃, 38 ℃and 41 ℃. It can be observed that the c-6A PEGPCL possesses a triple shape memory effect in the temperature of 38 and 41℃. In this polymer network, there exist two different units: the cross-linked PEG-PCL molecule chains and free PEG-PCL molecular chain. The cross-linked PEG-PCL regions with lower melting

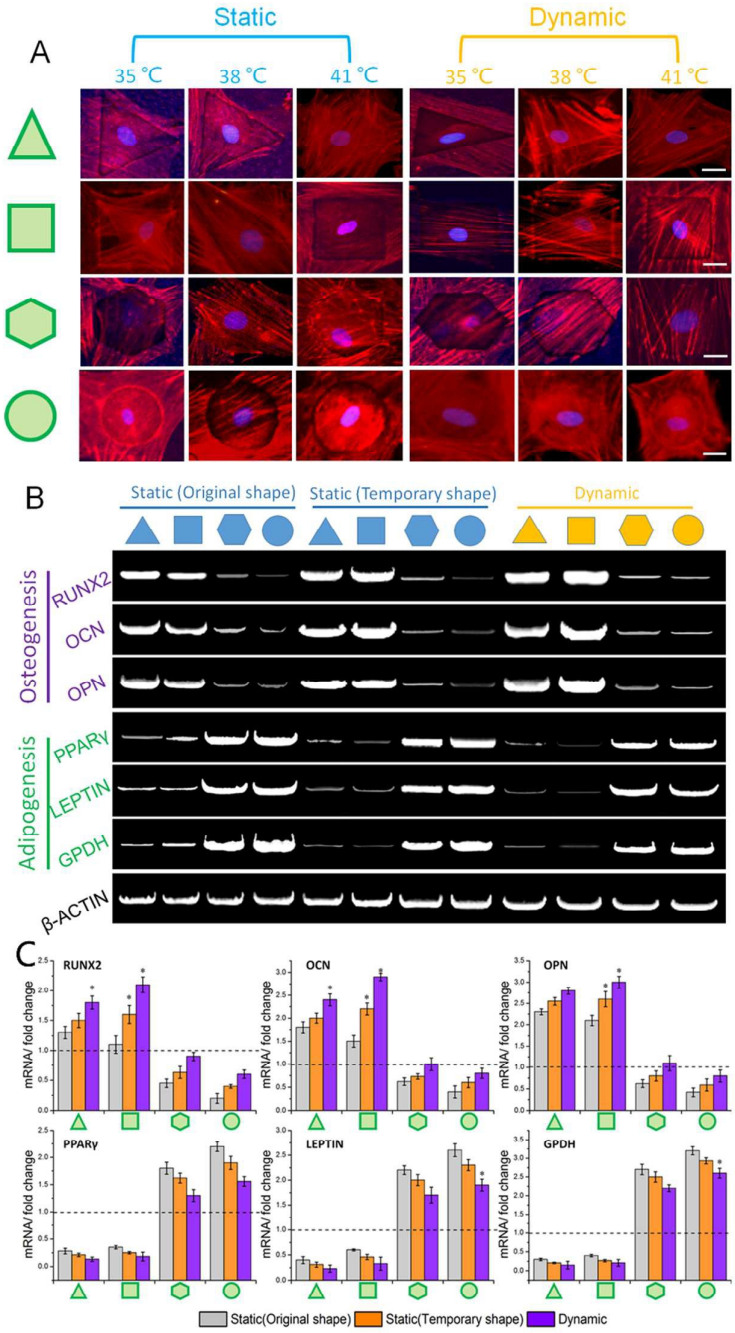

Figure 3. (A) Confocal laser scanning microscope images of immunostained cellular components (merged) for the rBMSCs, in which Rhodamine-Phalloidin labeled F-actin (red) and DAPI stained nuclei (blue) (Scale bar: 20 μm). These cells were cultured at days 2, 4, 6 post seeding, respectively, on such surfaces as static surface (dtatic-T, dtatic-S, static-H, and static-C) and dynamic surfaces including dynamic-T, dynamic-S, dynamic-H, and dynamic-C surfaces. (**B**) and (**C**) Relative gene level expression analyses of osteogenic (RUNX2, OCN and OPN), and adipogenesis (PPARγ, LEPTIN, and GPDH) markers. * p< 0.05, compared with static group.

temperature (T_{m1},38 ℃) triggered the first shape shifting by the low temperature and the free PEG-PCL segments determine the second shape shifting geometry due to the higher melting temperature (T_{m2}, 41°C).[40, 41]

As mentioned above, the c-6A PEGPCL has good SME on the macroscale near physiological temperature. To demonstrate whether the microwells have a microcosmic SME, the surface shape memory effect was carried out and observed by SEM. Microwells substrates containing an array of microwells with the same area (2000 μm^2) but different geometric forms (triangle, square, hexagon, and circle) were created using a thermal microimprint lithography technique. **Figure 2D** shows SEM images of dynamic topographic during shape recovery. When the temperature gradient increased, these different shape temporally microwells were almost recovered fully in a programmed mode. The surface microwells were deformed from the original shape to temporal shape by stretching the substrate, and were also fixed the deformed shape at 0℃ (**Scheme S1**). For example, the original shape of square was deformed from the length of side of 50 μm to long side of 94 μm, and the another side deformed from 50 μm to short side of 27 μm. However, the area and the angle of square were not changed. For the hexagon, the vertex angle was deformed from 60° to 43°. For the circle, the shape of microwells transformed from circle into ellipse. Upon reheating from 35℃ to 38, and 41℃, we can find that the temporally surface displayed a good shape memory with a recovery from an elongated geometrical shape to a series of recovered microwells. The square was recovered from the length of long side of 94 μm to 52 μm, and the another side recovered from 27 μm to 49 μm. For the hexagon, the vertex angle recovered from 43° to 53° and 59° for 38℃ and 41℃. For the circle, the shape of microwells transformed from ellipse into circle. During the recovery process, the depth and the area of these microwells were not changed (depth = 5 μm, Area=2000 μm^2). Therefore, we can draw a conclusion that the micrographics of c-6A PEGPCL have thermally SME near the body temperature and can be employed as a dynamic substrate to investigate the mechanism of stem cell differentiation in dynamic environment.

The *in vitro* degradation of the polymer films evaluated from the loss of the films and the reduction of the number average molecular weight of polymer is shown in **Figure S1** in SI. As shown in Figure S1A, the weight loss proceeded slowly during the entire degradation period. After 7 weeks of incubation, the c-6 A PEGPCL film lost approximately 90% of its initial mass. As shown in Figure S1B, the reduction of the molecular weight was faster than the mass loss of the samples, which was also consistent with the typical characteristic of bulk degradation. The degradation was attributed to the hydrolysis of the ester bonds of the PCL molecular chains.

Since the Elastic modulus of the material has a great influence on cell growth,[42] the stress–strain behaviors of c-6A PEG-PCL were measured at 35 °C, 38 °C and 41 °C, respectively (**Figure S2** in SI). With the temperature increased, the Young's moduli decreased gradually. The Young's moduli for this sample is about 15 MPa at 35 °C while it decreases to 13 MPa and 11.4 MPa for 38 °C and 41 °C. In this study, we chose the c-6A PEG-PCL (2000) substrate with the Young's modulus (or stiffness) of >10MPa to fabricate dynamically tunable surface micropatterns for cell growth. The reason is that it can mimic bone environment. [43,44]

3.3. Effect of dynamically tunable microwells on subcellular structure and differentiation of rBMSC

Significant efforts have addressed the role of the cytoskeletal structure in MSCs differentiation.[45, 46] To investigate the influence of cytoskeletal structure on dynamic microwells, the cytoskeletal structures before and after a programmed topographic transition were examined. After being cultured for 2, 4, and 6 d, rBMSCs on the static and dynamic microwells stained by DAPI and Rhodamine-phalloidin. As expected, after 2 d culture at 35℃, these cells were well localized and the shape of the cells in the microwells was highly modulated by the structures of the microwells (**Figure 3A**). When cultured on the static-Triangle (static-T) and static-Square (static-S) surfaces, rBMSCs were generally well spreading and the thick bundles of well-defined F-actin or stress fibers were observed. However, when the cell cultured on the static-Hexagon (static-H) and static-Circle (static-C), the thick bundles cannot be seen. The cells in the temporary microwells displayed an elongated shape and actin net-works self-organize into bundles comprising aligned long filaments, which were different from that of cells on the static

microwells surface. After 4 d culture, the cell shape gets shorter with the recovery of microwells. However, the cytoskeletal bundles still exist. In particular, the cytoskeletal bundle of dynamic square group (dynamic-S) is the most distinct. After 6 d culture, the temporary microwells recovered to the initial shape, and the cell shape changed from an elongated shape to the shape as the static microwells. However, the cytoskeletal structure has not changed with the change of microwells. It has been reported that actin cytoskeletal structure is a very important factor for MSC osteogenic differentiation, and the mechanical deformation can be translated by cytoskeleton reorganization into biochemical response because actin configuration is important in osteogenesis and the actin cytoskeleton can be used to predict if a cell is differentiating down an osteogenic pathway.[47, 48] As mentioned above that the dynamic micropatterns could play the significant roles in change cytoskeletal structure in the MSC microenvironment, we then investigated whether and how the dynamically tunable surface influences cell differentiation of rBMSCs.

rBMSCs have been shown to possess the propensity to differentiate along multiple lineages including osteogenesis and adipogenesis, which were our focuses in this work. To examine the degrees of differentiation of rBMSCs along these two lineages, we performed semi-quantitative PCR assays to analyze expression of the specific marker genes of rBMSCs after the 14 days culture. RUNX2, OCN and OPN were selected as the common osteogenic marker genes since their activations are known to coordinately regulate osteogenesis, while PPARγ, LEPTIN, and GPDH are chosen as the adipogenesis markers for the early, middle, and late differentiation stages, respectively. Compared to the static-H and static-C substrate, rBMSCs cultured on the static-T and static-S substrates expressed much more osteogenic genes, but much less adipogenic genes meanwhile. Inversely, rBMSCs displayed a strong adipogenic but weak osteogenic gene expression when cultured on the static-H and static-C substrates (**Figure 3B&C**). Cytoimmunofluorescence also revealed that rBMSCs of the static-T and static-S substrates expressed more abundant OCN proteins than another two groups (**Figure 4A**). These data indicated that rBMSC were induced to undergo osteogenesis by the triangle and square patterned culture surfaces but to adipogenesis by the hexon or round micropatterns.

Notably, it seems that the dynamically tunable alteration of the culture surface could promote rBMSCs to differentiate along osteogenesis while inhibit the adipogenesis (**Figure 3**). As shown in **Figure 3B&C**, all three genes which tightly control osteogenesis were further elevated in every group of rBMSC cultures upon subjection to the dynamically tunable alteration of the micropatterned surface. Compared to the hexon and circle groups, this elevation was significant and more dramatic than the triangle and square groups. In addition, OCN protein changed with a similar profile to its mRNAs (**Figure 4A**). Again, we observed that three adipogenic marker genes displayed an opposite change: their mRNA expression appeared to be conversely downregulated in all dynamic groups and this reduction was more prominent in both the hexon and circle groups than another two groups (**Figure 3B&C**). Interestingly, the upregulation of the selected osteogenic genes was the highest in the cells cultured on the dynamic-S among all of other cultures, suggesting that the dynamic-S might offer the more powerful signals directing rBMSCs to osteogenic differentiation.[49-52] To further confirm the effect of dynamic microwell patterning used in MSCs differentiation, semi-quantitative PCR assays to analyze the expression of specific marker genes of rBMSCs using traditional induction media and tissue culture polystyrene after the 14 days culture. As shown in **Figure S3** in SI, when adipogenic induction reagents were added into the culture medium, the adipogenic lineage was more obviously while the osteogenesis was further inhibited for 14 days culture. However, the osteogenesis lineage was more obvious when the adipogenic induction reagents were added into the culture medium. Interestingly, the degrees of rBMSCs differentiation on dynamic microwells patterning is approximate to the results of differentiation inducer group. Therefore, these dynamic microwells provide a potent tool to induce MSCs differentiation.

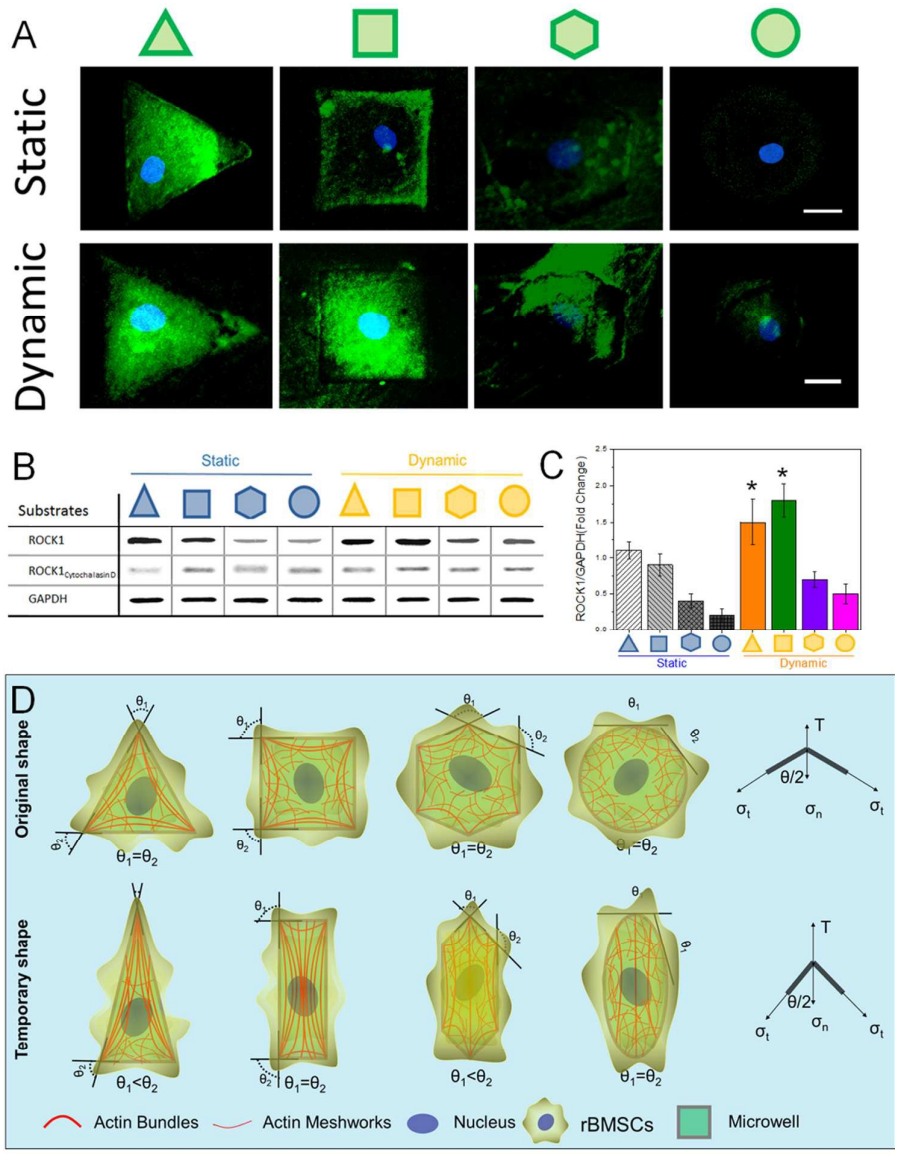

Figure 4. (A) Immunofluorescent images of cells cultured on such surfaces as static surface and dynamic surfaces for 14 days, and stained for OCN protein (green) and nuclei (blue). (**B**) and (**C**) protein quantitation of ROCK1(with and without Cytochalasin D) of rBMSCs cultured on such surfaces as static surface and dynamic surfaces without addition of any induction medium. **(D)** Schematic illustrating how different shape dynamic microwells accompanying with a dynamic changed local force from shape recovery affected cytoskeletal organization.

Since our studies above have shown that the dynamic microwells alter cytoskeletal structures and differentiation of rBMSC, we then focused on the effects of dynamically tunable surface on cell viability. As shown in **Figure S4** in SI, it was obvious that cell viability for all samples at the 2 day was more than 90%. After 4 days' and 6 days' cultivation, the cell viability on all group was more than 85%. To further confirm whether that microwells have negative effect on proliferation, the CCK8 assay was carried out. From **Figure S5** in SI, we can find that the cells on the dynamic and static microwells still have better proliferation activity compared with the control group.

To obtain more clues on whether the temperature changes affect MSCs growth, cell viability on the flat surface for different culture temperature was determined by means of the Alamar blue assay. As shown in **Figure S6**a, cell viability of the temperature variation groups was not decreased compared to the MSCs cultured either at 37℃ or at 35℃, which remained greater than 95%. From Figure S6b, it could be obviously seen that the MSCs were attached and

spread well on the flat substrates for all group. Thus, the temperature variation may play a little role in affecting the cell growth in this study.

3.4. The mechanism of rBMSC differentiation on dynamically tunable microwells

Recent studies show that the Rho-associated coiled coil-containing kinase (ROCK1) signaling axis, which is the major biochemical pathway mediating the actin cytoskeleton tension in non-muscle cells, plays a critical role in regulating survival and cloning efficiency of single MSCs.[53-56] RhoA is a member of Rho family small GTPases involved in cellular signaling and cytoskeletal organization, and it stimulates cytoskeleton tension through its effector, ROCK, which directly phosphorylates both nonmuscle myosin II (NMMII) regulatory myosin light chain (MLC) and MLC phosphatase to synergistically increase MLC phosphorylation and thus myosin II contractility.[26, 28, 57] Based on this finding, we analyzed the protein level of ROCK1 via Western blot (**Figure 4B&C**). It was observed that the rBMSCs on the static-T and static-S group substrate expressed the ROCK1 protein at a higher level to that on the static-H and static-C surface and the ROCK1 protein of static-T is the most distinct. In addition, ROCK1 was upregulated in cells on the dynamic substrate than the static substrate and the ROCK1 protein of dynamic-S is the most distinctly, indicating a close association of ROCK1 with the dynamic microwell-mediated cellular response. Cytochalasin D is a small molecule that inhibits F-actin polymerization and therefore reduces contractility of the actin cytoskeleton. Interesting, this agent removed the effect of cytoskeleton tension on differentiation but this time favored a ROCK1 decrease for cells on all patterning. Therefore, this cytoskeleton tension of cells is fully controlled by the patterns.

In the case of the static-microwells cells, the opening angle ϕ in **Figure 4D** is 60°, 90°, 120°, and 180° for Triangle, Square, Hexagon and Circle, respectively. When the cell stick on a sharp corner with opening angle ϕ, as shown in **Figure 4D**, the local force balance is given by

$$T = \sigma_n + 2\,\sigma_t \cos(\phi/2)$$

where σ_n acts along the bisecting line of the corner. Hence smaller the opening angle, the larger is the traction force (T).[58, 59] Stem cells sense and respond to changes of the local force of the ECM by modulating their endogenous cytoskeleton contractility. When the rBMSCs cultured on the static microwells, the largest static local force is static-T, followed by the static-S, static-H, and the smallest local force is static-C group.

Here we studied the actin cytoskeleton dynamics under dynamic geometrical and mechanical regulation from the 2D view. After deformation, the opening angle ϕ of the temporary micropatterns changed from 60°, 90°, 120°, and 180° to 47°, 90°, 43° and 180° for Triangle, Square, Hexagon and Circle, respectively. In addition, the other opening angles of Triangle and Hexagon increase. After thermal simulated topographic transition at 38°C, the opening angle ϕ in **Figure 4D** changed to 53°, 90°, 105°, and 180° for Triangle, Square, Hexagon and Circle micropatterns, respectively. At the same time, the dynamic local force of the Square and Circle was not changed and the dynamic local force of the Triangle and Hexagon decreased in the direction of deformation. Finally, the shape of microwells returned to the initial shape, and the local force decreased to the same quantity as the static group. In addition, a dynamic topographic transition is major constraint on activities in the cytoskeleton tension. For example, the ROCK1 protein of dynamic-S is the most distinctly. During the process of change of microwells, the actin bundles always exists and shows strong tension for all dynamic group.

In a word, the differentiation of cell cultured on the dynamic micropatterns was distinctive from the static surfaces, involving at least two factors, a topographic transition and a traction force between cell and the changing open angle ϕ in the process of shape recovery. In addition, the cytoskeleton organization is also affected by the local force between cell and the changing open angle ϕ in the process of shape recovery. When the dynamic micropatterns emerged and shrinked, cells were subjected to a convergent force while the width of micropattern decreased at the same time. For the dynamic-S and dynamic-C, the topographic transition could be more important or dominant compared to the traction force between cell and the changing open angle ϕ in the process of shape recovery. In the process of dynamic culture, the magnitude of the traction force remains unchanged between cell and the changing open angle ϕ on the dynamic-S and dynamic-C substrate because the changing open angle ϕ has no significant change in the process of shape recovery. As to dynamic-T and dynamic-H, cells on the dynamic micropatterns were

subjected to a decreasing force when the changing open angle ϕ increasing. In this time, the cytoskeleton tension can appear necessarily downtrend and the cytoskeleton bundles would be less.[60,61] Dynamic microwell cues can control stem cell differentiation by modulating the dynamic organization of cytoskeletal structure.

Considering our previous observation that the adherent rBMSCs on the triangle and square substrates had an increased cytoskeletal tension as shown by the elevation of ROCK1 (**Figure 4B&C**), and the previous studies revealing that the enhancement of cytoskeletal tension promotes osteogenesis,[46] it is as expected to see that rBMSCs were induced to differentiate along osteogenesis rather than adipogenesis by the culture on the triangle or square micro-well surfaces. Since the dynamic group of cells actually expressed the most ROCK1 proteins (**Figure 3B&C**) and showed the strongest cytoskeletal tension in the process of shape recovery, it is not surprising to observe the most dramatic induction of osteogenesis occurring in the mesenchymal stem cell exposed to the most vigorous cytoskeletal tension.

3.5. In vivo stem cell differentiation of dynamic microwells

To further confirm if the dynamic microwells could regulate stem cell differentiation *in vivo* and look into their effects on bone repair and regeneration, mandible bone defects were created in the rabbits and the deformed microwell films were implanted into the defected sites (**Figure S7** in SI). Heating were given by applying hot packs to the microwell films to recover their temporary shapes to their original ones *in vivo*. Three months later, animals were killed and the defected sites were examined with Masson staining to see the repair efficacy of mandible bone defects *in vivo*.

In consistent with their osteogenic inducibility demonstrated *in vitro*, the administration of the static-T and static-S types of microwell films generated obvious new bone appearing near the defect sides, and the mature bone trabeculae were formed at the defect areas (**Figure 5B**). When the dynamic microwell films were applied, much more new bone formation was defected with the most significant increase in the new bone percentage brought by the dynamic tunable alteration of the square microwell film as expected (**Figure 5A-C**). In turn, we detected much less new bone tissues and no mature bone trabecular in the defect areas implanted with the static-H and circle type of

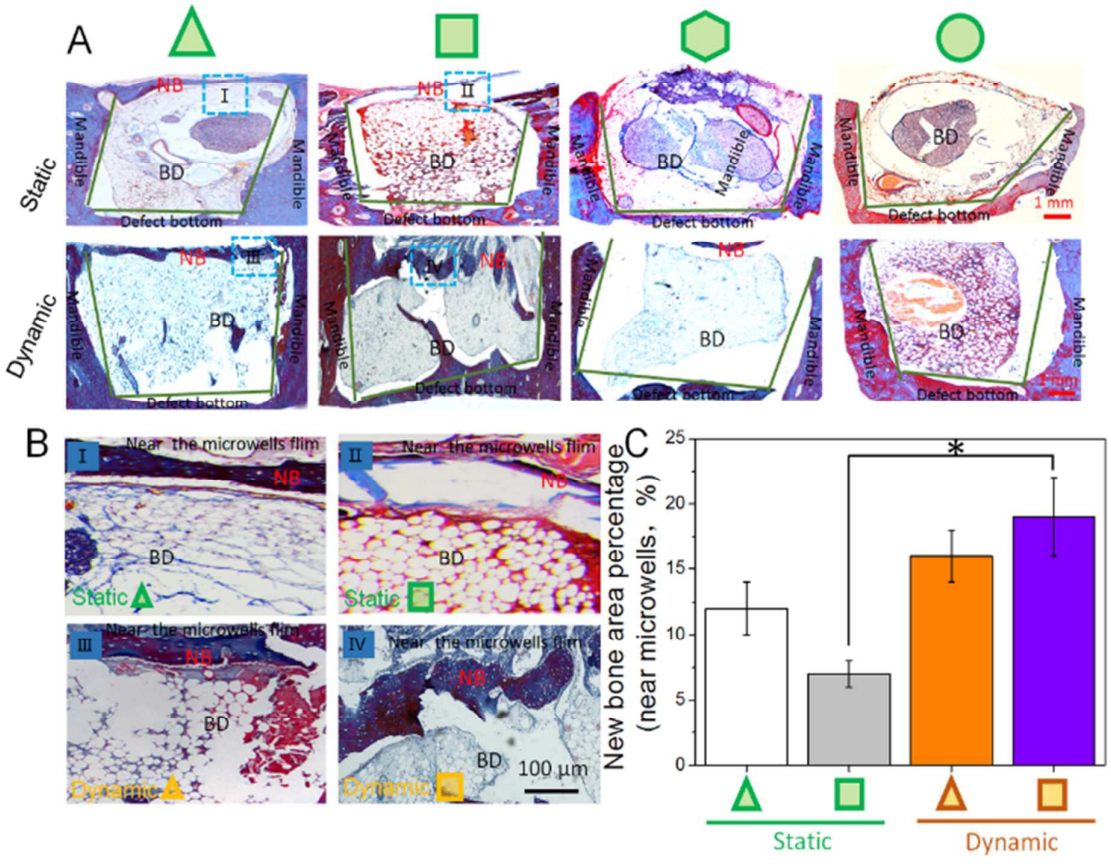

Figure 5. (A) Histomorphometric results of the bone defect area (BD: Bone defect; NB: New Bone), ; (**B**) High magnification of Masson staining near the geometric microwells, which showed that many multinuclear cells were found around the films (Ⅰ -Ⅳ correspond to the dash squares of (A)); and (**C**) Quantification of the histological. * $p < 0.05$, compared with Static-S group.

films (**Figure 5A**); the defect areas were loose, full of granulation tissues and filled with blue staining collagen fibers, indicating that the wounded bone was still in repairing and the regeneration of bone was delayed or attenuated. Additionally, only the Square type of film yielded a slight increase in new bone formation by the dynamic treatment (**Figure 5B**). These results suggested that the geometric shape of the static-T and static-S could improve bone formation compared to the static-H and static-C, and the dynamic tuning of the microwells could further benefit bone regeneration *in vivo*.

At last, we further quantified the neonatal bone in the defect areas at 8 weeks to demonstrate the effects of the dynamic microwells on new bone formation (**Figure 5B & C**). Significant difference was found between the static-S and dynamic-S, with an improved repair efficacy by the dynamic microwells compared to the static group. Considering that the premature bone mineralization were found to be mainly located near the films, we expect a better repair performance in the bone defect once a 3D microwell scaffold is applied.

Conclusions

In summary, we demonstrate the dynamic structural signals resulting from the micro-well substrates to guide the rat bone marrow mesenchymal stem cells. The micro-well substrates, which were made of 6A PEGPCL polymer with excellent biocompatible, biodegradable and thermally activated shape memory function, were fabricated via thermal lithography with different shape arrays. The dynamically tunable geometric microwells and the resulting the mechanical force effectively and significantly regulated the cytoskeletal structure and tension of rBMSC *in vitro* without induction media when compared with the static patterned. The traction force between cell and the changing open angle ϕ is decreased gradually due to the shape recovery as temperature increases from 35 ℃ to 41 ℃, leading to the dynamic reorganization of cytoskeletal structure. Cellular and molecular analyses revealed that cells cultured in various dynamic micro-wells had disparately differentiated along adipogenesis and osteogenesis pathways. More importantly, the *in vivo* result demonstrated that the dynamically tunable polymer microwells possessed a capacity of prompting mesenchymal stem cells to differentiate along osteogenesis and in turn efficiently repair the mandible bone defect. Therefore, this work can provide a potent tool to explore cell response to complex micromechanical environments and may be of great potential for applications in tissue engineering.

Acknowledgements

This work was partially supported by National Basic Research Program of China (973 Program, 2012CB933600) and National Natural Science Foundation of China (51173150, 51373138), National Key Project of Scientific and Technical Supporting Programs Funded by MSTC (2012BAI17B06), Research Fund for the Doctoral Program of Higher Education of China (20120184110029) and Construction Program for Innovative Research Team of University in Sichuan Province (14TD0050).

References

1.D. Odde, *Cell*, 2011, **144**, 325-326.
2.W. L. Murphy, T. C. McDevitt and A. J. Engler, *Nat. Mater.*, 2014, **13**, 547-557.
3.D. Dado, M. Sagi, S. Levenberg and A. Zemel, *Regen. Med.*, 2012, **7**, 101-116.
4.D. E. Ingber, *Proc. Natl. Acad. Sci. U.S.A.*, 2005, **102**, 11571-11572.
5.J. T. Connelly, J. E. Gautrot, B. Trappmann, D. W. Tan, G. Donati, W. T. S. Huck and F. M. Watt, *Nat. Cell. Biol.*, 2010, **12**, 711-718.
6.C. S. Chen, *Science*, 1997, **276**, 1425-1428.
7.D. E. Discher, D. J. Mooney and P. W. Zandstra, *Science*, 2009, **324**, 1673-1677.
8.A. J. Engler, S. Sen, H. L. Sweeney and D. E. Discher, *Cell*, 2006, **126**, 677-689.
9.P. M. Gilbert, K. L. Havenstrite, K. E. G. Magnusson, A. Sacco, N. A. Leonardi, P. Kraft, N. K. Nguyen, S. Thrun, M. P. Lutolf and H. M. Blau, *Science*, 2010, **329**, 1078-1081.
10.M. J. Dalby, N. Gadegaard, R. Tare, A. Andar, M. O. Riehle, P. Herzyk, C. D. W. Wilkinson and R. O. C. Oreffo, *Nat. Mater.*, 2007, **6**, 997-1003.
11.T. D. Pollard and J. A. Cooper, *Science*, 2009, **326**, 1208-1212.
12.J. T. Parsons, A. R. Horwitz and M. A. Schwartz, *Nat. Rev. Mol. Cell. Bio.*, 2010, **11**, 633-643.
13.D. A. Fletcher and R. D. Mullins, *Nature*, 2010, **463**, 485-492.
14.R. Peng, X. Yao and J. Ding, *Biomaterials*, 2011, **32**, 8048-8057.
15.K. A. Kilian, B. Bugarija, B. T. Lahn and M. Mrksich, *Proc. Natl. Acad. Sci. U.S.A.*, 2010, **107**, 4872-4877.
16.J. Fu, Y. Wang, M. T. Yang, R. A. Desai, X. Yu, Z. Liu and C. S. Chen, *Nat. Methods.*, 2010, **7**, 733-736.
17.E. K. F. Yim, E. M. Darling, K. Kulangara, F. Guilak and K. W. Leong, *Biomaterials*, 2010, **31**, 1299-1306.
18.P. Lu, K. Takai, V. M. Weaver and Z. Werb, *Csh.*

Perspect. Biol., 2011, **3**, a5058.
19.P. Lu, V. M. Weaver and Z. Werb, *J. Cell. Biol.*, 2012, **196**, 395-406.
20.R. McBeath, D. M. Pirone, C. M. Nelson, K. Bhadriraju and C. S. Chen, *Dev. Cell.*, 2004, **6**, 483-495.
21.A. J. Engler, C. Carag-Krieger, C. P. Johnson, M. Raab, H. Y. Tang, D. W. Speicher, J. W. Sanger, J. M. Sanger and D. E. Discher, *J. Cell. Sci.*, 2008, **121**, 3794-3802.
22.A. Buxboim and D. E. Discher, *Nat. Methods.*, 2010, **7**, 695-697.
23.L. Adamo, O. Naveiras, P. L. Wenzel, S. McKinney-Freeman, P. J. Mack, J. Gracia-Sancho, A. Suchy-Dicey, M. Yoshimoto, M. W. Lensch, M. C. Yoder, G. García-Cardeña and G. Q. Daley, *Nature*, 2009, **459**, 1131-1135.
24.J. Holst, S. Watson, M. S. Lord, S. S. Eamegdool, D. V. Bax, L. B. Nivison-Smith, A. Kondyurin, L. Ma, A. F. Oberhauser, A. S. Weiss and J. E. J. Rasko, *Nat. Biotechnol.*, 2010, **28**, 1123-1128.
25.C. Galli, M. Piemontese, S. Lumetti, F. Ravanetti, G. M. Macaluso and G. Passeri, *Acta. Biomater.*, 2012, **8**, 2963-2968.
26.Y. Sun, C. S. Chen and J. Fu, *Annu. Biophys.*, 2012, **41**, 519-542.
27.K. Kurpinski, J. Chu, C. Hashi and S. Li, *Proc. Natl. Acad. Sci. U.S.A.,* 2006, **103**, 16095-16100.
28.Y. L. Han, S. Wang, X. Zhang, Y. Li, G. Huang, H. Qi, B. Pingguan-Murphy, Y. Li, T. J. Lu and F. Xu, *Drug. Discov. Today.*, 2014, **19**, 763-773.
29.N. Shimizu, K. Yamamoto, S. Obi, S. Kumagaya, T. Masumura, Y. Shimano, K. Naruse, J. K. Yamashita, T. Igarashi and J. Ando, *J. Appl. Physiol.*, 2008, **104**, 766-772.
30.F. Chowdhury, S. Na, D. Li, Y. Poh, T. S. Tanaka, F. Wang and N. Wang, *Nat. Mater.*, 2009, **9**, 82-88.
31.J. Li, S. Vadahanambi, C. Kee and I. Oh, *Biomacromolecules*, 2011, **12**, 2048-2054.
32.L. Huang, X. Zhuang, J. Hu, L. Lang, P. Zhang, Y. Wang, X. Chen, Y. Wei and X. Jing, *Biomacromolecules*, 2008, **9**, 850-858.
33.P. Miaudet, A. Derre, M. Maugey, C. Zakri, P. M. Piccione, R. Inoubli and P. Poulin, *Science*, 2007, **318**, 1294-1296.
34.A. Lendlein and S. Kelch, *Angew. Chem. Int. Ed.*, 2002, **41**, 2034.
35.T. Gong, K. Zhao, W. Wang, H. Chen, L. Wang and S. Zhou, *J.Mater. Chem. B*, 2014, **2**, 6855-6866.
36.S. Zhou, X. Deng and H. Yang, *Biomaterials*, 2003, **24**, 3563-3570.
37.T. Gong, W. Li, H. Chen, L. Wang, S. Shao and S. Zhou, *Acta Biomater*, 2012, **8**, 1248-1259.
38.T. Gong, K. Zhao, G. Yang, J. Li, H. Chen, Y. Chen and S. Zhou, *Adv Healthc Mater*, 2014, **3**, 1608-1619.
39.J. Kim, W. Bae, H. Choung, K. T. Lim, H. Seonwoo, H. E. Jeong, K. Suh, N. L. Jeon, P. Choung and J. H. Chung, *Biomaterials*, 2014, **35**, 9058-9067.
40.M. Y. Razzaq, M. Behl, K. Kratz and A. Lendlein, *Adv Mater*, 2013, **25**, 5514-5518.
41.S. Pandini, S. Passera, M. Messori, K. Paderni, M. Toselli, A. Gianoncelli, E. Bontempi and T. Riccò, *Polymer*, 2012, **53**, 1915-1924.
42. R. Peng, X. Yao, B. Cao, J. Tang and J. Ding, *BIOMATERIALS*, 2012, **33**, 6008-6019.
43. M. P. Staiger, A. M. Pietak, J. Huadmai and G. Dias, *BIOMATERIALS*, 2006, **27**, 1728-1734.
44. F. Kantawong, K. E. V. Burgess, K. Jayawardena, A. Hart, M. O. Riehle, R. O. Oreffo, M. J. Dalby and R. Burchmore, *ACTA BIOMATER*, 2010, **6**, 3694-3703.
45.P. S. Mathieu and E. G. Loboa, *Tissue. Eng. Part. B-Rev*, 2012, **18**, 436-444.
46.T. Vignaud, L. Blanchoin and M. Théry, *Trends. Cell. Biol.*, 2012, **22**, 671.
47.C. M. Kirschner and K. S. Anseth, *Small*, 2013, **9**, 578-584.
48.M. Thery, *J. Cell. Sci.*, 2010, **123**, 4201-4213.
49.X. Yao, R. Peng and J. Ding, *Biomaterials*, 2013, **34**, 930-939.
50.J. Lee, A. A. Abdeen and K. A. Kilian, *Sci Rep*, 2014, **4**, 5188.
51.J. Fouchard, C. Bimbard, N. Bufi, P. Durand-Smet, A. Proag, A. Richert, O. Cardoso and A. Asnacios, *Proc. Natl. Acad. Sci. U.S.A*, 2014, **111**, 13075-13080.
52.D. Wang, W. Zheng, Y. Xie, P. Gong, F. Zhao, B. Yuan, W. Ma, Y. Cui, W. Liu, Y. Sun, M. Piel, W. Zhang and X. Jiang, *Sci. Rep.*, 2014, **4**, 6160.
53.B. Hu, W. Shi, Y. Wu, W. R. Leow, P. Cai, S. Li and X. Chen, *Adv. Mater.*, 2014, **26**, 5786-5793.
54.M. Guvendiren and J. A. Burdick, *Nat. Commun.*, 2012, **3**, 792.
55.S. F. M. van Dongen, P. Maiuri, E. Marie, C. Tribet and M. Piel, *Adv. Mater.*, 2013, **25**, 1687-1691.
56.U. S. Schwarz and M. L. Gardel, *J. Cell. Sci.,* 2012, **125**, 3051-3060.
57.A. Hall, *Science*, 1998, **279**, 509-514.
58.S. Banerjee and M. Cristina Marchetti, *New. J. Phys.*, 2013, **15**, 35015.
59.A. Brock, E. Chang, C. C. Ho, P. LeDuc, X. Jiang, G. M. Whitesides and D. E. Ingber, *Langmuir*, 2003, **19**, 1611-1617.
60. T. Chen, C. Wu, M. Tang, J. Huang and F. Su, *PLOS ONE*, 2010, **5**, e14392.
61. C. M. Kraning-Rush, S. P. Carey, J. P. Califano, B. N. Smith and C. A. Reinhart-King, *PHYS BIOL*, 2011, **8**, 15009.

The dynamically tunable geometric microwells has a great capacity of regulating the cytoskeletal structure and differentiation of mesenchymal stem cells along adipogenesis and osteogenesis pathways.